Phase diagram of colloidal spheres in a biaxial electric or magnetic field

Frank Smallenburg[a] and Marjolein Dijkstra
Soft Condensed Matter, Debye Institute for Nanomaterials Science, Utrecht University, Princetonplein 5, Utrecht 3584 CC, The Netherlands

(Received 19 October 2009; accepted 14 April 2010; published online 28 May 2010)

Colloidal particles with a dielectric constant mismatch with the surrounding solvent in an external biaxial magnetic or electric field experience an "inverted" dipolar interaction. We determine the phase behavior of such a system using Helmholtz free energy calculations in Monte Carlo simulations for colloidal hard spheres as well as for charged hard spheres interacting with a repulsive Yukawa potential. The phase diagram of colloidal hard spheres with inverted dipolar interactions shows a gas-liquid transition, a hexagonal ABC stacked crystal phase, and a stretched hexagonal-close-packed crystal. The phase diagram for charged spheres is very similar, but displays an additional layered-fluid phase. We compare our results with recent experimental observations. [doi:10.1063/1.3425734]

I. INTRODUCTION

The phase behavior of colloidal particles in a suspension can be influenced by applying an oscillating external magnetic or electric field. If the magnetic susceptibility or dielectric constant of the colloidal particles differs from that of the solvent, the particles will acquire a dipole moment along an external uniaxial field, leading to dipolar interactions between the particles. In this way, the colloidal interactions can be tuned reversibly without having to modify the chemistry of the colloidal particles or the solvents involved. Hence, an external uniaxial electric or magnetic field leads to a greater control over the macroscopic phase behavior and structure of the colloidal system. The phase behavior of both hard and charged colloids with aligned dipolar interactions obtained by applying an external uniaxial field has been studied theoretically[1,2] and experimentally[3–6] extensively. In addition, the phase diagram of charged and uncharged dipolar hard spheres has been determined by free energy calculations using Monte Carlo simulations.[7] In this work, it was shown that three new crystal structures, i.e., hexagonal-close-packed (hcp), body-centered-tetragonal, and body-centered-orthorhombic phases, can be stabilized by applying an external uniaxial field. For completeness, we mention that the behavior of colloidal particles with permanent dipole moments in external fields[8–10] and in confinement[11,12] has been widely investigated as well.

By applying multiaxial fields, more complicated anisotropic interactions can be induced, leading to the formation of more complex particle structures.[13] In this paper, we determine the phase diagram of colloidal particles in an external biaxial electric or magnetic field, which can be obtained by rotating or randomly changing the field direction. Effectively, the particles have a rotating dipole moment in the plane of the rotating field. If the frequency of the rotating field is sufficiently high, the particles experience a rotationally or time averaged dipolar interaction, leading to a net attraction in the plane of the biaxial field, and a repulsion perpendicular to the field. The time-averaged dipolar interaction that the particles experience in a uniaxial field rotating in the xy-plane is just $-1/2$ times the dipolar interaction in a uniaxial field oriented in the z-direction, and can be regarded as a negative or "inverted" dipolar interaction. In contrast to the relatively simple dipolar interaction, the inverted dipolar interactions between the colloids give rise to a gas-liquid coexistence at low field strengths. At higher field strengths, large hexagonal sheets of particles form, eventually merging into a crystal phase.

Simulations of particles in various biaxial and multiaxial fields have been performed by Martin *et al.*,[13–16] with a focus on kinetics and nonequilibrium structures, as well as magnetic properties of the structures formed. The magnetic properties have also been compared to experimental results measured in systems of magnetic field-structured composites, formed by polymerizing the solvent while the particles are in the external field.[17] In a study of freely rotating permanent dipoles in a rotating field, Murashov and Patey[18] showed the formation of sheetlike and layered structures for a range of angular velocities of the external field, using molecular dynamics and Brownian dynamics simulations. In these systems, the formation of layers highly depends on the moment of inertia of the dipoles and the frequency of the rotating field. More recently, colloidal systems in an external biaxial electric field have been investigated using confocal microscopy,[19] showing the formation of large hexagonal sheetlike structures, which were made permanent by thermal annealing. The formation of these sheets in two-dimensional systems has also been studied experimentally[20] with the particles confined to an interface. In this paper, we investigate using Monte Carlo simulations the equilibrium phase behavior of charged and uncharged colloidal hard spheres interacting with an inverted dipolar interaction. Additionally, we map out the phase diagrams for both systems using free energy calculations.

[a]Electronic mail: f.smallenburg@uu.nl.

II. METHODS

We perform Monte Carlo simulations in the canonical (*NVT*) and isothermal-isobaric (*NPT*) ensemble, where we fix the volume V and pressure P, respectively. In addition, we keep the number of particles N in the system fixed and the temperature T. We perform simulations of $N=384-432$ particles. Larger systems were used for the layered-fluid phase and the low-density crystals to reduce finite-size effects. Finite size effects were checked by performing the same free energy calculation in a larger system ($N=900$) at one point in each phase diagram. This caused the fluid-solid coexistence packing fractions to shift by less than 0.005 in both the charged and uncharged system, which remains within our statistical error bars.

Cluster moves were introduced to move or rotate clusters of particles at once in order to speed up equilibration of the layered-fluid phase. In the initial step of a cluster move, a random particle in the system is selected and taken as the center of the cluster. We construct a cylindrical volume around this particle with its symmetry axis aligned along the z-axis. The radius r_c and height h are selected randomly from a uniform distribution. For our simulations, we use $0<r_c<\min(L_x,L_y)$ and $0<h<\sigma$. All particles positioned with their center of mass in the cylinder are considered to be part of the cluster and are moved collectively. In the case of a rotation move, the particles are rotated around the central particle in the plane of the external field. In the case of a translation move, the particles are given the same random displacement $d\mathbf{r}$. The number of particles in the cluster volume is counted before and after the cluster move. If any new particles are present in the cluster volume after the move, moving the same cluster in reverse would also move these extra particles. As this would break detailed balance, any cluster moves where the number of particles in the chose cylinder around the central particle changes are rejected. Eventually, the translation or rotation is accepted or rejected based on the Boltzmann factor $\exp(-\beta(U_{\text{new}}-U_{\text{old}}))$.

In our model, we assume an external rotating electric or magnetic field in the xy-plane of our system. The colloidal particles experience an inverted dipolar interaction given by

$$\beta u_{inv}(\mathbf{r}_{ij}) = -\frac{\gamma}{4}\left(\frac{\sigma}{r_{ij}}\right)^3 (1-3\cos^2\theta_{ij}), \tag{1}$$

where $\mathbf{r}_{ij}$ is the center-of-mass distance vector between particles i and j, θ_{ij} denotes the angle that $\mathbf{r}_{ij}$ forms with the z-axis, σ is the diameter of the particle, and $\beta=1/k_BT$ with k_B Boltzmann's constant. In the case of an external electric field $\mathbf{E}$, the dimensionless prefactor γ in Eq. (1) is given by

$$\gamma = \frac{\pi\alpha^2\epsilon_s\sigma^3|\mathbf{E}|^2}{8k_BT}, \tag{2}$$

where $\alpha=(\epsilon_p-\epsilon_s)/(\epsilon_p+2\epsilon_s)$ is the dielectric contrast factor with $\epsilon_{p,s}$ the dielectric constants of the particles and the solvent, respectively. Similarly, in the case of an external magnetic field $\mathbf{H}$, γ is written as

$$\gamma = \frac{\pi\alpha^2\mu_s\sigma^3|\mathbf{H}|^2}{8k_BT}, \tag{3}$$

where $\alpha=(\mu_p-\mu_s)/(\mu_p+2\mu_s)$ and $\mu_{p,s}$ is the magnetic susceptibilities of the particles and the solvent, respectively. We note that for $\gamma=1$, the maximum value of the pair potential, i.e., $0.5k_BT$, is reached, when two adjacent particles are aligned along the z-axis. The minimum value ($-0.25k_BT$) is obtained when both adjacent particles are in the xy-plane. In addition, the colloidal hard spheres interact with a hard-sphere potential given by

$$\beta u_{hs}(r_{ij}) = \begin{cases} 0, & r_{ij} \geq \sigma \\ \infty, & r_{ij} < \sigma \end{cases} \tag{4}$$

while we use a repulsive hard-core Yukawa potential in the case of charged spheres

$$\beta u_Y(r_{ij}) = \begin{cases} \dfrac{\epsilon \exp[-\kappa(r_{ij}-\sigma)]}{r_{ij}/\sigma}, & r_{ij} \geq \sigma \\ \infty, & r_{ij} < \sigma \end{cases}, \tag{5}$$

where

$$\epsilon = \frac{Z^2}{(1+\kappa\sigma/2)^2}\frac{\lambda_B}{\sigma} \tag{6}$$

is a constant prefactor depending on the colloidal charge number Z, Debye screening length κ^{-1}, and Bjerrum length $\lambda_B=e^2/\epsilon_s k_BT$ with e the elementary charge. Equation (5) is the pair potential given by the Derjaguin–Landau–Verwey–Overbeek theory for charged colloids.[21] We have neglected the van der Waals attraction in Eq. (5) as we are interested in refractive index matched systems. The repulsion increases the distance between the layers of the crystal phase, and causes part of the liquid phase to form fluidlike layers.

The Ewald summation is employed to calculate the long-range dipolar interactions.[22,23] The calculation of the inverted dipolar interactions using the Ewald summation method is largely identical to the method used for normal dipolar systems, with the exception of the term related to the boundary conditions. In this case, we assume conducting boundary conditions. We first note that the inverted dipolar interaction, which is formed by a time-averaged rotating dipolar interaction in the xy-plane, is identical to the averaged interaction induced by two perpendicular external uniaxial fields in the xy-plane. Hence, the total potential energy of the system is the average of two energy calculations. The correction factor can be derived by summing the effect of the boundary conditions on both of these calculations.

For nonconducting boundary conditions, the total potential energy of a specific configuration $\{\mathbf{r}^N\}$ of the inverted dipolar system U_{inv}^{nc} equals the average of the total potential energy of two dipolar systems with uniaxial fields in the x and y directions

$$U_{inv}^{nc} = \frac{U_x^{nc}+U_y^{nc}}{2} = -\frac{1}{2}U_z^{nc}. \tag{7}$$

For normal dipolar interactions the difference between nonconducting and conducting boundary conditions is given by[22]

$$U_{x,y,z}^{\mathrm{cond}} = U_{x,y,z}^{nc} - \frac{2\pi}{3V}\mathbf{M}\cdot\mathbf{M}, \tag{8}$$

where U^{cond} is the interaction with conducting boundary condition and $\mathbf{M}$ is the square of the total dipole moment of the system, with $\mathbf{M}\cdot\mathbf{M}=\gamma N^2/2$. Combining the difference in potential energy between conducting and nonconducting boundary conditions for the two dipolar systems with perpendicular uniaxial fields, yields

$$\begin{aligned} U_{inv}^{\mathrm{cond}} &= \frac{U_x^{\mathrm{cond}} + U_y^{\mathrm{cond}}}{2}, \\ &= \frac{U_x^{nc} + U_y^{nc}}{2} - \frac{2\pi}{3V}\frac{\gamma N^2}{2}, \\ &= -\frac{1}{2}U_z^{nc} - \frac{2\pi}{3V}\frac{\gamma N^2}{2}, \\ &= -\frac{1}{2}U_z^{\mathrm{cond}} - \frac{\pi}{V}\frac{\gamma N^2}{2}. \end{aligned} \tag{9}$$

As a result, we can calculate the potential energy of a biaxial system with conducting boundary conditions U_{inv}^{cond} from the energy of the same configuration in a system with normal dipolar interactions by multiplying the energy by $-1/2$ and adding the above correction term $-\pi\gamma N^2/2V$.

The Helmholtz free energies of the ABC stacked crystals were calculated using the Einstein integration method.[22,24] In addition, we calculate the Helmholtz free energy as a function of density by integrating the equation of state. We determine the coexisting densities with the fluid phase by employing the common tangent construction. At high densities, a coexistence between face-centered-cubic (fcc) and hcp crystal phases occurs. The free energy difference between these structures is on the order of $10^{-3}k_BT$, and therefore hard to measure with sufficient statistical accuracy using this method. Instead, we use the hard-sphere crystal as a reference state for both structures, and calculate the free energy as a function of the interaction strength by using a thermodynamic integration path consisting of a gradual increase in the field strength. For these crystals, only the free energy difference between hcp and fcc stacking is needed, which was linearly interpolated from literature values for this difference at coexistence and close packing.[25] Due to the narrow coexistence region, and a large estimated error in the free energy calculations, we only show one coexistence line between these high-density crystal phases. The estimated error in the coexistence field strength γ is on the order of 0.5. For the fluid phase, the hard-sphere fluid (using the equation of state by Speedy[26]) and ideal gas were used as reference states for the liquid and the gas, respectively.

For the free energy of the layered-fluid phase in the case of charged spheres, we use a method similar to the one employed by Bolhuis and Frenkel[27] for the smectic phase of hard spherocylinders. Via a thermodynamic integration path, we relate the free energy of the layered fluid in the system of charged spheres with inverted dipolar interactions to the free energy of a hard sphere fluid. This integration is done in two steps. We first couple the particles to their layers by applying an external sinusoidal potential while turning off the interactions. The resulting potential in the system depends on a switching coefficient λ

$$U(\lambda) = \lambda U_{\mathrm{sin}} + (1-\lambda)U_{\mathrm{int}} \tag{10}$$

$$= \lambda\alpha\sum_{i=0}^{N}\sin(2\pi n_l z_i/L_z) + (1-\lambda)U_{\mathrm{int}}, \tag{11}$$

with U_{sin} and U_{int} the total energy in the system due to the external potential and the particle interactions, respectively. The factor α is the strength of the sinusoidal potential and is chosen such that the particles in the layer remain disordered for all $0<\lambda<1$. The number of layers n_l and the height of the box L_z are chosen such that they match the equilibrium layer spacing measured from independent NPT simulations. The free energy difference between $F_{\mathrm{inv}}-F_{\mathrm{sin}}$ the system with inverted dipolar interactions and the system with the sinusoidal potential is given by

$$\beta(F_{\mathrm{inv}} - F_{\mathrm{sin}}) = \int_1^0 d\lambda\langle U_{\mathrm{sin}} - U_{\mathrm{int}}\rangle_\lambda - \ln V. \tag{12}$$

The resulting system consists of hard spheres confined to layers by the external potential. To allow equilibration of the density within the layers throughout the whole system, we use shifted boundary conditions, such that the fluid layers are interconnected at the edges of the simulation box. In our simulation, a particle that leaves the simulation box in the x-direction does not only enter the simulation box at the opposite face, but is also shifted in the z-direction by one fluid layer, i.e., by L_z/n_l. The direction of the shift is determined by the direction in which the particle leaves the simulation box. In this way, the particles can diffuse throughout the whole system, as there is effectively one single layer, which allows for the relaxation of the density within each fluid layer. Of course, the energy calculations should also incorporate this shift. For the Yukawa interaction and the real space contribution of the Ewald sums, this can be done by simply calculating the energy from the relevant image particles. For the reciprocal space contribution of the Ewald summation, we use the fact that the system is still periodic along x, but with a period n_l times larger and with n_l times more particles. Since the contributions from these extra particles are the same as those in the original box, but multiplied by a complex factor, the energy calculation does not require significant extra computer time.

The free energy of the system of pure hard spheres in an external sinusoidal potential can be calculated in two ways. Turning off the potential, the system transforms gradually into an isotropic hard-sphere fluid, which can be used as a reference state. The free energy difference between the hard sphere fluid and hard spheres in an external sinusoidal potential can be calculated similar to Eq. (12), but without inverted dipolar interactions. Combining the two steps, the free energy of the layered fluid can then be calculated as

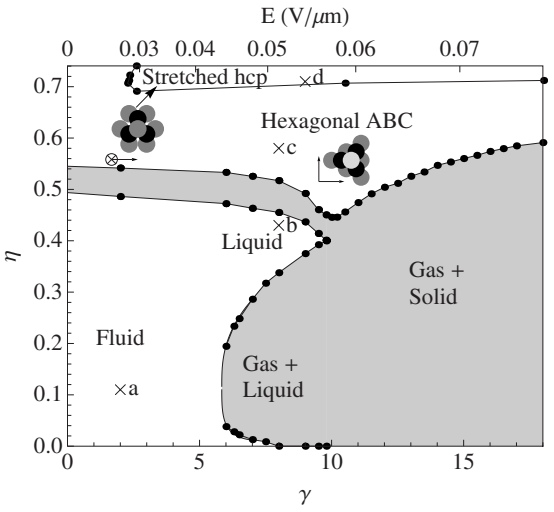

FIG. 1. Phase diagram for hard spheres in an external biaxial electric or magnetic field in the dipole moment strength γ vs packing fraction η representation. The black circles denote the points where the phase boundaries were determined, while the gray areas denote the coexistence regions. The tielines that connect the coexisting phases are vertical. The hexagonal ABC stacked crystal phase can be regarded as a fcc crystal, which is stretched in the direction perpendicular to the field and is oriented with the hexagonal planes parallel to the plane of the biaxial field, as illustrated by the two perpendicular arrows indicating the plane of the field in the schematic picture. The stretched hcp is oriented with the hexagonal planes perpendicular to the biaxial field, as illustrated by the ⊗ and arrow in the picture, with ⊗ indicating the axis perpendicular to the page, and is slightly stretched in the direction perpendicular to the field. The top axis shows the electric field strength corresponding to the dipole moment strength γ, using the experimental values $\alpha=-0.22$, $\epsilon_s=5.8\epsilon_0$, $\sigma=2$ μm, and $T=300$ K (Ref. 19). The crosses denote the points where the snapshots in Fig. 2 were taken.

$$\beta F_{\text{inv}} = \beta F_{\text{HS}} + \int_0^1 d\lambda \langle U_{\text{sin}} \rangle_\lambda^{\text{HS}} + \int_1^0 d\lambda \langle U_{\text{sin}} - U_{\text{int}} \rangle_\lambda$$

with F_{HS} the free energy of a hard sphere fluid at the same density as the layered fluid, and with the first integral evaluated without inverted dipolar interactions. Alternatively, if the strength of the external sinusoidal potential is sufficiently high, the particles are strongly constrained to their layer and the system behaves effectively as a two-dimensional hard-disk fluid with additional harmonic vibrations perpendicular to the plane, for which one can calculate the free energy analytically. We checked that the free energies using both methods are equal within our statistical error bars. However, since integrating to a hard sphere fluid uses a shorter integration path, the numerical errors in this method are smaller. Note that two integration paths are needed: In the first path, we switch off the inverted dipolar interactions, but we have to switch on an external sinusoidal potential to keep the symmetry of the fluid. In the second path, we turn off the sinusoidal potential to obtain a homogeneous fluid phase.

III. HARD SPHERES IN A BIAXIAL FIELD

We plot the calculated phase diagram for hard spheres in a biaxial field in Fig. 1. In Fig. 2, we show snapshots of the system in various phases, as denoted by the crosses in the phase diagram (Fig. 1). At $\gamma=0$, the well-known hard-sphere fluid-fcc (hexagonal ABC stacked) phase behavior is recovered. As opposed to the normal dipolar hard spheres,[7] we

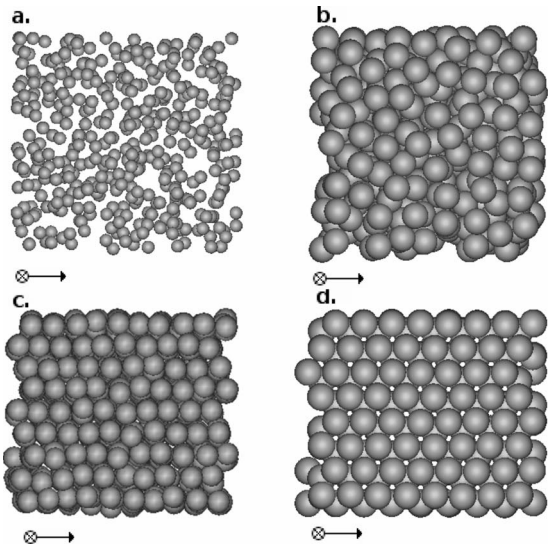

FIG. 2. Snapshots of typical simulation configurations for hard spheres with inverted dipolar interactions. The arrows indicate the two field directions, with ⊗ indicating the axis perpendicular to the page. (a) A low-density fluid at $\gamma=2$, $\eta=0.11$. (b) A higher density fluid, with $\gamma=8$ and $\eta=0.43$. (c) Crystalline ABC-stacked hexagonal layers of spheres at $\eta=0.58$ and $\gamma=8$. (d) The stretched hcp crystal at $\gamma=9$, $\eta=0.71$. Note that the stretched hexagonal planes are perpendicular to the field plane.

find at $\gamma \simeq 6$ a gas-liquid coexistence for this system. We note that well-inside the gas-liquid coexistence region, system-size spanning slabs of liquid and gas are formed, which are aligned in the plane of the rotating field. Moreover, the system can phase separate and/or change phase very easily. It is tempting to speculate that these observations are due to a strongly anisotropic gas-liquid interfacial tension, which is much lower for the plane parallel to the biaxial field than the orthogonal planes.

Additionally, we find two stable crystal structures in the phase diagram. At maximum packing the fcc crystal is favored for low field strengths due to the small free energy difference between fcc and hcp, where fcc is the most stable phase in the case of hard spheres ($\gamma=0$). The orientation of the crystal phase with respect to the field has no effect on its energy when the crystal is not deformed, however, at nonzero field strengths, the crystal is compressed in the plane of the field and stretched in the perpendicular direction, leading to a difference in free energy between the possible orientations for the crystal. As a result, the stable structure consists of hexagonal sheets parallel to the field plane.

The lowest-energy structure of this system is a close-packed hcp crystal, with the hexagonal planes perpendicular to the plane of the rotating field. The energy per particle for this orientation $[-1.481\ 38(1)\gamma kT]$ is slightly lower than that of hcp with sheets oriented parallel to the field $[-1.480\ 12(1)\gamma kT]$ or that of fcc $[-1.480\ 96(1)\gamma kT$, for any orientation]. Evidently, the free energy difference between fcc and hcp is very small for the different orientations, and hcp is only stable in a small pocket at very high densities. At lower densities, the stable structure is fcc. We wish to remark here that the fcc and the hcp phases are not entirely symmetric, but are slightly stretched in the z-direction. Hence, the fcc phase is an ABC-stacked crystal of hexagonal sheets,

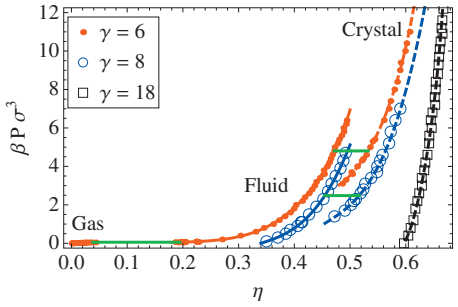

FIG. 3. Equations of state for hard spheres with inverted dipolar interactions at field strengths $\gamma=6,8,18$. The lines are fits through the data, using dashed lines for the crystals and solid lines for the fluids. The green horizontal lines show the coexistences. For $\gamma=8$ and 18 the coexistences with a gas at near-zero pressure have been omitted.

oriented along the xy-plane, while in the hcp phase the hexagonal planes themselves are stretched. Stacking defects are likely to occur, since the free energy loss is only on the order of $10^{-3}kT\gamma$ per particle at close packing, and becomes even lower at lower densities.

Solitary sheets or rafts can appear at high field strengths whenever there are insufficient particles in the simulation box to form a box-spanning sheet. However, if the fields are strong enough to form these structures, and there are multiple sheets in the box, they will join into a crystal if their orientation matches, showing that these structures are not stable on their own. Our phase diagram explains these findings as it displays indeed an enormous widening of the solid-gas transition for increasing γ. We note that the tielines that connect the coexisting phases are vertical in Fig. 1. Hence, the coexisting gas and solid phases becomes progressively more dilute and dense, respectively, upon increasing γ, yielding coexistence of a dense solid phase with a gas phase, which is extremely dilute.

Equations of state for the fluid and fcc phases at field strengths $\gamma=6,8,18$ are shown in Fig. 3. For $\gamma=6$, a gas, liquid, and solid branch are shown, with the coexistences denoted by horizontal lines. For $\gamma=8$, only the liquid and solid branch are shown, as the liquid coexists with a gas at near zero density. At $\gamma=18$, we show only the fcc branch, which again coexists with an extremely dilute gas.

IV. CHARGED SPHERES IN A BIAXIAL FIELD

The colloidal particles that are used in experimental systems are often charged, due to ionizable groups on their surfaces, which dissociate when suspended in a solvent. The bare Coulombic repulsions between the colloidal particles are then screened by the ions in the solvent, leading to a Yukawa or screened-Coulombic interaction.[21] In our simulations, we choose an inverse screening length of $\kappa\sigma=10$, and surface charge $Z^2\lambda_B/\sigma=450$. The phase diagram for charged spheres in an external biaxial field is shown in Fig. 4. Figure 5 shows snapshots of the system at the points denoted by crosses in the phase diagram. In Fig. 6 we show the equations of state for three field strengths. For $\gamma=10$, the fluid and crystal branch are shown. At $\gamma=16$, the liquid and solid branch are shown, omitting the coexistence with a gas at near

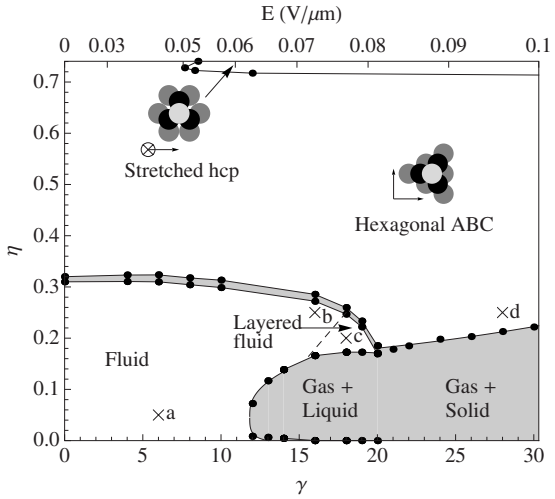

FIG. 4. Same as Fig. 1, but for a system of charged spheres interacting with a Yukawa interaction. The inverse screening length $\kappa\sigma=10$, and $\lambda_B Z^2/\sigma=450$ ($\epsilon=12.5$). The layered-fluid phase consists of system-spanning slabs of fluid aligned in the plane of the biaxial field. The crosses indicate the positions in the phase diagram where the snapshots in Fig. 5 were taken.

zero pressure. For $\gamma=24$, we again show only the crystal branch, which also coexists with a gas at extremely low pressures.

At $\gamma=0$, we find a fluid-fcc (hexagonal ABC) coexistence with coexisting packing fractions $\eta_{\text{fluid}}=0.31$ and $\eta_{\text{fcc}}=0.32$. Additionally, we again find a gas-liquid coexistence, which is shifted to much lower densities compared to that of hard spheres. Moreover, the coexisting liquid becomes inhomogeneous for field strengths $\gamma>16$, and system-size spanning fluidlike layers are formed with their orientations aligned in the plane of the rotating field. Figure 5(c) shows a

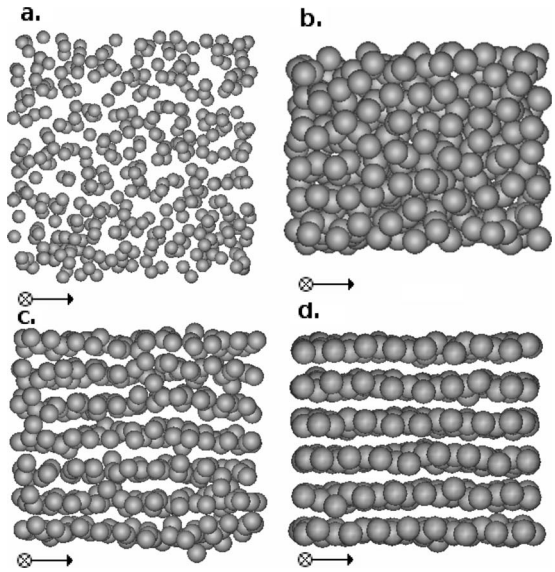

FIG. 5. Snapshots of typical simulation configurations for charged spheres with inverted dipolar interactions. The arrows indicate the two field directions, with ⊗ indicating the axis perpendicular to the page. (a) A low-density fluid at $\gamma=6$, $\eta=0.05$. (b) A higher density fluid, just above the line in the phase diagram marking the crossover between the homogeneous and layered fluids ($\gamma=16$, $\eta=0.26$). (c) Layered fluid at $\gamma=18$, $\eta=0.20$. (d) Crystalline ABC-stacked hexagonal layers of charged spheres at $\eta=0.32$ and $\gamma=28$.

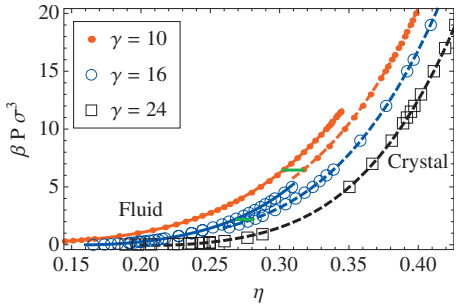

FIG. 6. Equations of state for charged spheres with inverted dipolar interactions at field strengths $\gamma=10,16,24$. The lines are fits through the data, using dashed lines for the crystals and solid lines for the fluids. The green horizontal lines show the coexistences. Both the crystal at $\gamma=24$ and the liquid at $\gamma=16$ also coexist with an extremely dilute gas at near-zero density.

typical configuration of a layered-fluid phase. The inhomogeneous structure of the fluid phase can be explained by the Yukawa repulsion between the particles, which not only increases the distances between the particles within each sheet, but also induces a repulsion between neighboring sheets. Particles can diffuse from one layer to another, but close to the triple point, this process slows down significantly. In addition, we also observe large fluctuations in the distances between adjacent sheets at low pressures, indicating a low free energy cost to create an interface between the gas and the layered-fluid phase. Consequently, at low densities the system can easily form small numbers of fluid layers, which are separated by a dilute gas phase. It is likely that the same would happen in experiments at low packing fractions, especially when the sheets are too large to move easily. At low field strengths, a stable homogeneous liquid exists in between the layered-fluid phase and the stable crystal phase, but disappears when $\gamma>19$. The transition between the layered-fluid phase and the isotropic liquid appears to be continuous as no hysteresis can be seen in the equation of state, and the amplitude in the density profile of the layers changes continuously with field strength and density. Exemplarily, Fig. 7 displays the pair correlation function that measures the positional order in the direction perpendicular to the field for varying packing fractions. We indeed observe clearly that the amplitude decreases continuously with increasing packing fraction.

The lowest energy state of the system now depends on the field strength: At close packing and $\gamma>5.9168(2)$, the

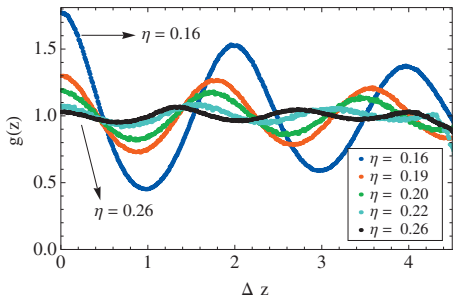

FIG. 7. Pair correlation function in the z-direction (perpendicular to the biaxial field) of the layered-fluid phase with dipole moment strength $\gamma=17$ for varying packing fractions. The amplitude decreases with increasing η, as denoted by the labels.

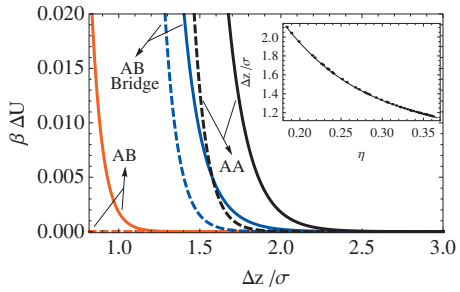

FIG. 8. Difference in potential energy per particle $\Delta\beta U$ between a perfect crystal of ABC stacked hexagonal sheets and differently stacked sheets, at $\gamma=30$ as a function of the center-to-center distance between the sheets Δz. From left to right, the red, blue, and black solid lines denote the comparison with AB hollow-site stacking, AB bridge-site stacking, and AA stacking, respectively. The dashed lines represent the contributions from the Yukawa interactions to the total potential energy difference. The inset shows the sheet distance as a function of the packing fraction at $\gamma=30$.

dipolar interactions dominate the Yukawa interactions, and hcp is the ground state. At lower field strengths, the Yukawa interactions cause the system to favor the fcc phase. Due to the entropy difference for hard spheres between fcc and hcp [$0.0011(1)kT$ per particle at close packing[25]], the phase transition between the two structures appears at slightly higher field strength than $\gamma=5.9168$, i.e., $\gamma=8.4(4)$. We again note that the hexagonal planes of the fcc and hcp phase are parallel and perpendicular, respectively to the plane of the biaxial field (xy-plane) and that both structures are stretched in the z-direction. Hence, the fcc phase is a hexagonal ABC stacked crystal phase, and the hcp is a slightly stretched hcp phase.

We also find that the coexistence region between a dilute gas phase and the ABC stacked crystal becomes wider upon increasing γ. However, the density of the crystal at coexistence is much lower than in the hard sphere case, mainly due to a larger distance between adjacent sheets [as shown in Fig. 5(d)]. As the distance between the sheets increases, the effect of the relative position and orientation between neighboring sheets on the potential energy reduces significantly, leading to a large amount of disorder in the position and orientation of the sheets. We observe that the distance between the sheets can fluctuate significantly during our simulations at low densities. However, the crystal is still the stable phase. In the bulk limit, the entropy gain from detaching a sheet from the crystal would be dominated by the energy cost to detach an infinite sheet of particles. Consequently, the fcc crystal will be the thermodynamically stable phase in the bulk limit. In finite systems, however, the sheets will be translationally and rotationally disordered. The translational disorder can be clearly seen to appear in simulations: When a crystal phase is used as the initial configuration, the layers of the crystal become disordered during simulations at low density. Rotational disorder does not emerge in crystals in a rectangular periodic box, but is expected to appear in experimental setups. At low pressures, the separations between the hexagonal sheets fluctuate substantially, resulting in large density fluctuations. It is likely that these fluctuations contribute to the disorder of the sheets as well.

In Fig. 8, we plot the difference in potential energy per

particle $\beta\Delta U$ of various stackings of the hexagonal crystalline sheets in the crystal phase with ABC stacking, as a function of sheet distance Δz for $\gamma=30$. In addition, we plot the contribution of the Yukawa interaction to this potential energy difference, denoted by the dashed lines, and we observe that the contribution from the dipolar interaction dominates that of the Yukawa interaction close to coexistence. We find that the total difference in potential energy decreases exponentially with sheet distance. The potential differences are dominated by the dipolar repulsions from nearby particles in the adjacent layer. Hence, hollow-site stackings have the lowest potential energy, while the AA stacking corresponds to the highest one. In the inset, we plot typical sheet separations Δz for equilibrium ABC stacked crystals close to the coexistence density. In the inset, we plot typical sheet separations Δz for equilibrium ABC stacked crystals close to the coexistence density. We find that at a sheet distance of $\Delta z = 2.0\sigma$, the difference in potential energy per particle between ABC and AA stacking is only $0.002k_BT$ per particle, while the difference compared with other stackings is even smaller. As a result, we expect large amounts of stacking disorder in any low-density crystal.

V. COMPARISON WITH EXPERIMENTS

Recently, colloidal systems in an external biaxial field have been studied experimentally by Leunissen *et al.*[19] In these experiments, a biaxial field was applied by using two perpendicular uniaxial electric fields and randomly changing the field direction. A system of colloids in suspension with large amounts of salt was used in order to approach the uncharged case. Field strengths were varied in a range approximately corresponding to $31<\gamma<170$, and the packing fraction was $\eta=0.2$. The particles were seen to organize into large hexagonal sheets, with multiple domains, which generally did not merge into three-dimensional structures due to orientational disorder. However, close to the edge of the sample, where the orientation of the hexagonal structure was fixed by the wall, they observed an AB bridge-site stacking of the sheets, which is in contradiction with our bulk simulations. Even in the case of charged particles, where we find substantial disorder between the sheets, there is a clear preference for hollow-site stacking of the particles, as can be seen in Fig. 8. As our simulations do not take into account the effect of the walls, it seems likely that the walls in the experiments impose an orientation on the hexagonal planes. If the walls attract the particles, they will also cause the layers to be translationally aligned in the direction perpendicular to the wall. This would mean the sheets can only move relative to their neighbors along the direction parallel to both the wall and one of the field directions. In this case, an AB bridge-site stacking would indeed be the lowest-energy state (Fig. 8 illustrates the potential energy difference between AB bridge-site stacking and AA stacking). Further from the wall, no stacking preference was clearly visible, which indeed agrees with the disorder seen in the simulations. In the experimental setup, the sheets are much larger than in the simulations, which slows down their motion considerably. In addition, the sheets can have multiple domains with different orientations, and can be attached to the walls or other sheets, further preventing equilibration.

VI. CONCLUSIONS

In conclusion, we have calculated the phase diagrams for uncharged and charged hard spheres in an external biaxial electric or magnetic field. In both systems, the interaction included a hard-core interaction and an inverted dipolar interaction with its strength determined by the field strength γ. In the charged sphere case, a Yukawa repulsion was included as well, using $\kappa\sigma=10.0$ and $\lambda_B Z^2/\sigma=450$. The phase behavior as a function of the field strength and particle density shows a gas-liquid coexistence for both systems, as well as a number of crystal structures. All crystal structures found are distortions of the close-packed structures hcp and fcc, where the distortions are caused by a stretching of the crystal in the direction perpendicular to the plane of the biaxial field. Especially in the case of charged spheres, these deformation can be very strong, resulting in separations between layers of particles on the order of 2σ. While free energy considerations show that even at low densities the stable crystal structure is that of fcc, we expect a huge number of planar defects present in the crystal as the potential energy differences are small. In addition to these structures, the system of charged spheres exhibits a layered-fluid phase close to the triple point. These layers are internally disordered, but the density profiles show strong periodicity perpendicular to the plane of the rotating field.

[1] B. Groh and S. Dietrich, Phys. Rev. E **63**, 021203 (2001).
[2] S. Klapp and F. Forstmann, Phys. Rev. E **60**, 3183 (1999).
[3] A. Yethiraj and A. van Blaaderen, Nature (London) **421**, 513 (2003).
[4] A. Yethiraj, J. H. J. Thijssen, A. Wouterse, and A. van Blaaderen, Adv. Mater. **16**, 596 (2004).
[5] T. Chen, R. N. Zitter, and R. Tao, Phys. Rev. Lett. **68**, 2555 (1992).
[6] U. Dassanayake, S. Fraden, and A. van Blaaderen, J. Chem. Phys. **112**, 3851 (2000).
[7] A.-P. Hynninen and M. Dijkstra, Phys. Rev. Lett. **94**, 138303 (2005).
[8] G. M. Range and S. H. L. Klapp, J. Chem. Phys. **122**, 224902 (2005).
[9] S. Klapp, J. Phys.: Condens. Matter **17**, R525 (2005).
[10] J. Jordanovic and S. H. L. Klapp, Phys. Rev. Lett. **101**, 038302 (2008).
[11] S. H. L. Klapp and M. Schoen, J. Chem. Phys. **117**, 8050 (2002).
[12] S. H. L. Klapp and M. Schoen, J. Mol. Liq. **109**, 55 (2004).
[13] J. E. Martin, R. A. Anderson, and R. L. Williamson, J. Chem. Phys. **108**, 3765 (1998).
[14] J. E. Martin, R. A. Anderson, and R. L. Williamson, J. Chem. Phys. **108**, 7887 (1998).
[15] J. E. Martin, R. A. Anderson, and C. P. Tigges, J. Chem. Phys. **110**, 4854 (1999).
[16] J. E. Martin, R. A. Anderson, and R. L. Williamson, J. Chem. Phys. **118**, 1557 (2003).
[17] J. E. Martin, E. Venturini, J. Odinek, and R. A. Anderson, Phys. Rev. E **61**, 2818 (2000).
[18] V. V. Murashov and G. N. Patey, J. Chem. Phys. **112**, 9828 (2000).
[19] M. E. Leunissen, H. R. Vutukuri, and A. van Blaaderen, Adv. Mater. **21**, 3116 (2009).
[20] N. Elsner, C. P. Royall, B. Vincent, and D. R. E. Snoswell, J. Chem. Phys. **130**, 154901 (2009).
[21] B. Derjaguin and L. Landau, Acta Physicochim. URSS **14**, 633 (1941); E. J. W. Verwey and J. Th. G. Overbeek, *Theory of the Stability of Lyotropic Colloids* (Elsevier, Amsterdam, 1948).

[22] D. Frenkel and B. Smit, *Understanding Molecular Simulations*, 2nd ed. (Academic, London, 2002).
[23] P. P. Ewald, Ann. Phys. **369**, 253 (1921).
[24] D. Frenkel and A. J. C. Ladd, J. Chem. Phys. **81**, 3188 (1984).
[25] P. G. Bolhuis, D. Frenkel, S. C. Mau, and D. A. Huse, Nature (London) **388**, 235 (1997).
[26] R. J. Speedy, J. Phys.: Condens. Matter **9**, 8591 (1997).
[27] P. Bolhuis and D. Frenkel, J. Chem. Phys. **106**, 666 (1997).